

Supporting Information for

Polyoxometalate-Based Metal-Organic Frameworks for Selective Oxidation of Aryl Alkenes to Aldehydes

Yuanyuan Ma,[†] Haiyue Peng,[†] Jianing Liu,[†] Yonghui Wang,^{*†} Xiuli Hao,^{†,‡} Xiaojia Feng,^{†,⊥} Shifa Ullah Khan,[†] Huaqiao Tan,^{*†} and Yangguang Li^{*†}

[†] Key Laboratory of Polyoxometalate Science of the Ministry of Education, Faculty of Chemistry, Northeast Normal University, Changchun, 130024, China. E-mail: liyg658@nenu.edu.cn; tanhq870@nenu.edu.cn.

[‡] School of Chemical and Biological Engineering, Taiyuan University of Science and Technology, Taiyuan 030021 (P.R. China)

[⊥] College of Science, Shenyang Agricultural University, Shenyang, 110866, P.R. China

section	page
Characterization methods	S2
X-ray Crystallography	S2
Supplementary figures for compounds 1 and 2	S3
Supplementary tables for compounds 1 and 2	S13
Reference	S16

1. Characterization Methods

Elemental analyses of C, H and N elements were performed on a Perkin-Elmer 2400 CHN elemental analyzer. W and Co were determined by a Leaman Inductively Coupled Plasma (ICP) spectrometer. Alpha Centaur FT/IR spectrophotometer with pressed KBr pellets was employed to record the IR spectra ranging from 4000-400 cm^{-1} . The TG analyses were carried out under N_2 atmosphere flow by employing a SDT Q600 TG instrument with a heating rate of 10 $^\circ\text{C min}^{-1}$. The powder X-ray diffraction (PXRD) patterns were collected by using a Smart Lab X-Ray diffractometer with $\text{Cu-K}\alpha$ ($\lambda = 1.5418 \text{ \AA}$) radiation in the 2θ range from 5° to 50° at a scanning rate of 2° per minute. The GC analyses were performed on Agilent Technologies 7820A GC system equipped with a flame ionization detector (FID) and a capillary column (J & W HP-5, 30 m x 0.32 mm). Identification of the products was conducted by $^1\text{H-NMR}$ and $^{13}\text{C NMR}$ spectroscopy (Bruker INOVA-500) and comparing the NMR spectral data with those of the commercially available pure substances.

2. X-ray Crystallography

Single-crystal X-ray diffraction data for compounds 1-2 were collected by using a Bruker Smart Apex CCD diffractometer with $\text{MoK}\alpha$ radiation ($\lambda = 0.71073 \text{ \AA}$) at the temperature of 298(2) K. All structures were solved by the direct method and refined by a full-matrix least-squares method on F^2 using the SHELXTL-2018 crystallographic software package.^[1] All non-hydrogen atoms were refined anisotropically. The hydrogen atoms on organic carbon atoms were fixed in calculated positions. Hydrogen atoms on water molecules which cannot be assigned from the weak reflection peaks were directly included into the final molecular formula. Furthermore, the restraint command "ISOR" was used to restrain non-H atoms with ADP and NDP problems in compounds 1-2. Moreover, the triazole and benzene rings of the BBTZ ligands in these two compounds were also restrained with the commands "AFIX 69", "AFIX 59", "DELU", and "DFIX" so as to restrain the bond distance and angles of organic ligands with a chemically reasonable structural features. In the final refinement, both compounds exhibit solvent accessible voids but no lattice water molecules can be clearly assigned from the weak residual peaks. Thus, the SQUEEZE program was further used to remove the contributions of weak reflections to the whole data. The new generated hkl files were further used to refine the final crystal data of 1 and 2. Based on the elemental analysis, TG analysis, charge-balance consideration and the SQUEEZE calculation results, ten lattice water molecules are directly included in the final molecular formula of compound 1. One nitrate anion (NO_3^-) and four lattice water molecules are added in the molecular formula of compound 2. Crystal data and structural refinement for 1-2 are listed in Table 4. Selected bond lengths and angles of 1-2 are listed in Table S2 and S4.

3. Supplementary figures for compounds 1 and 2.

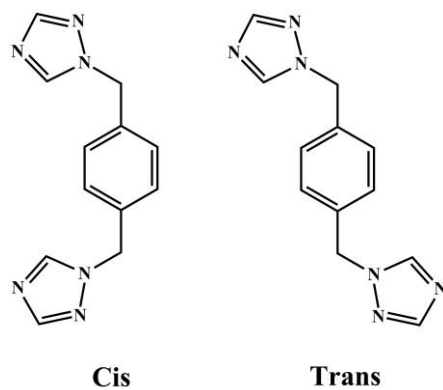


Figure S1 Two configurations of BBTZ.

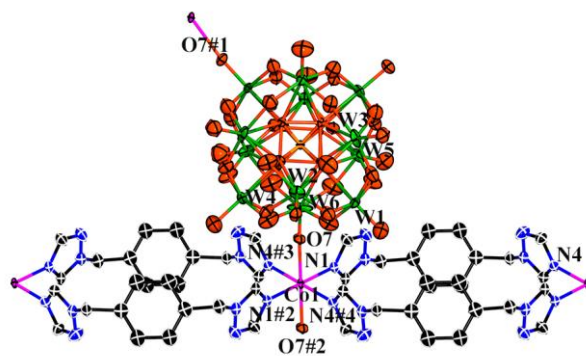


Figure S2 ORTEP diagram of the basic structural units in compound 1 with thermal ellipsoids at 30% probability displacement. (symmetry codes: #1 $-x,y,-z+3/2$; #2 $-x+1/2,-y+3/2,-z+2$; #3 $x-1/2,y-1/2,z$; #4 $-x+1,-y+2,-z+2$; #5 $x+1/2,y+1/2,z$).

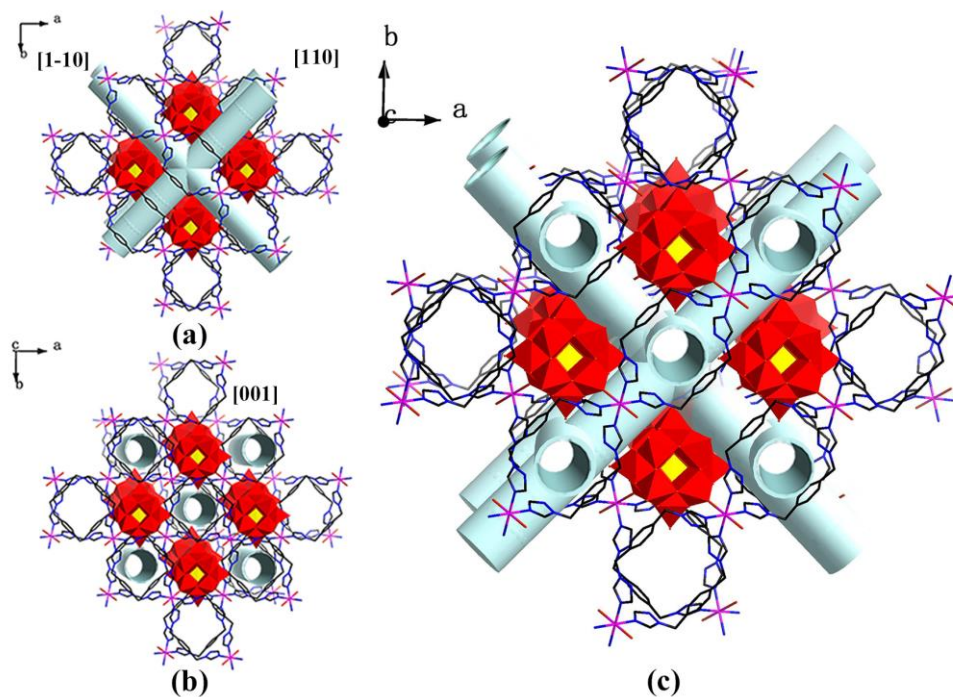


Figure S3 (a-c) Ball-and-stick and polyhedral view of the three-dimension open structure of compound 1 with three directional channels. Blue channels in (a) represent the channels run along $[110]$ and $[1-10]$ direction, and the channels are inter-connected along ab plane. The blue channel in (b) represents the channels run along $[001]$ direction. The channels in (c) show the channel systems intersect with each other and run three different directions.

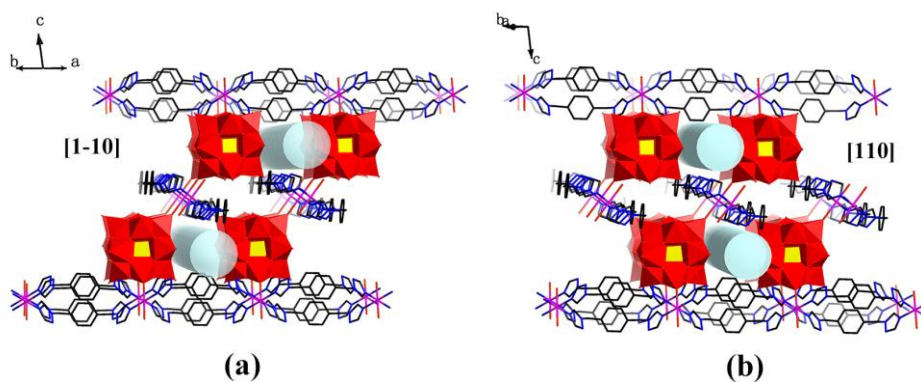


Figure S4 (a) The channels in compound 1 running along $[1-10]$ direction. (b) the channels in compound 1 running along $[110]$ direction. .

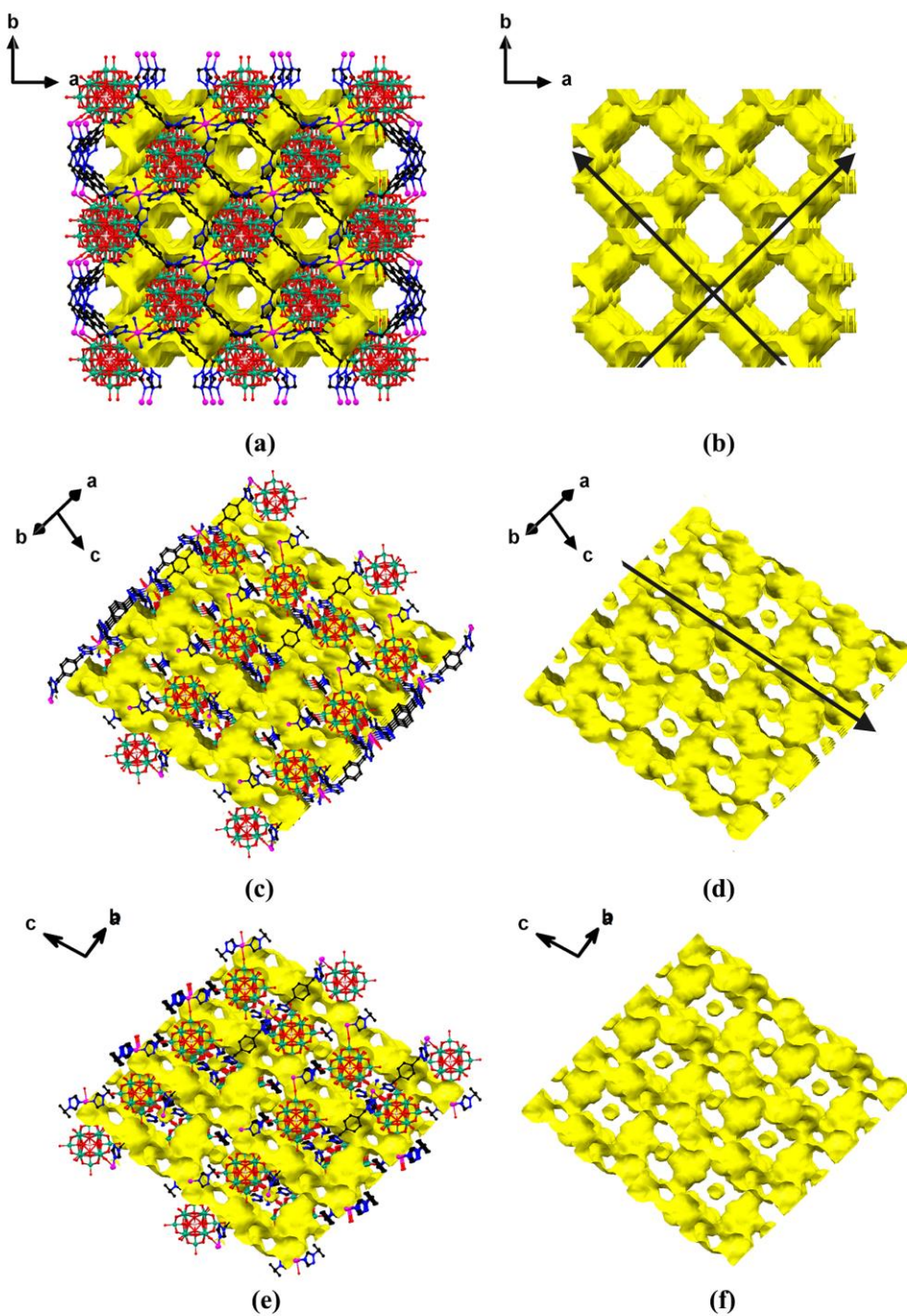


Figure S5 (a-f) Packing arrangement of compound 1, in which the solvent accessible voids in the three-directional channels are modeled with yellow background: (a) and (b) viewed along [001] direction; (c) and (d) viewed along [1-10] direction; (e) and (f) viewed along [110] direction.

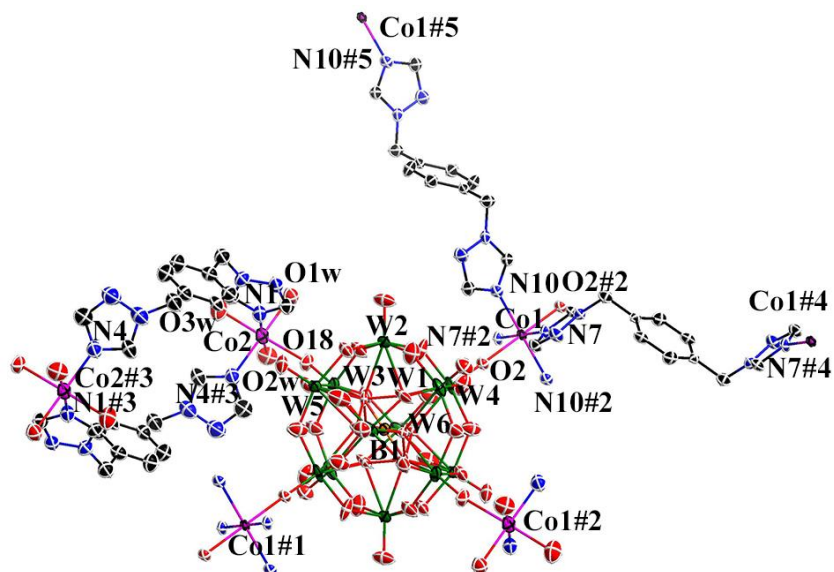


Figure S6 ORTEP diagram of the basic structural units in compound 2 with thermal ellipsoids at 30% probability displacement. (symmetry codes: #1 $-x+1,-y+1,-z+1$; #2 $-x,-y+1,-z+1$; #3 $-x+2,-y+1,-z+2$; #4 $-x,-y+2,-z+1$; #5 $-x,-y+1,-z+2$)

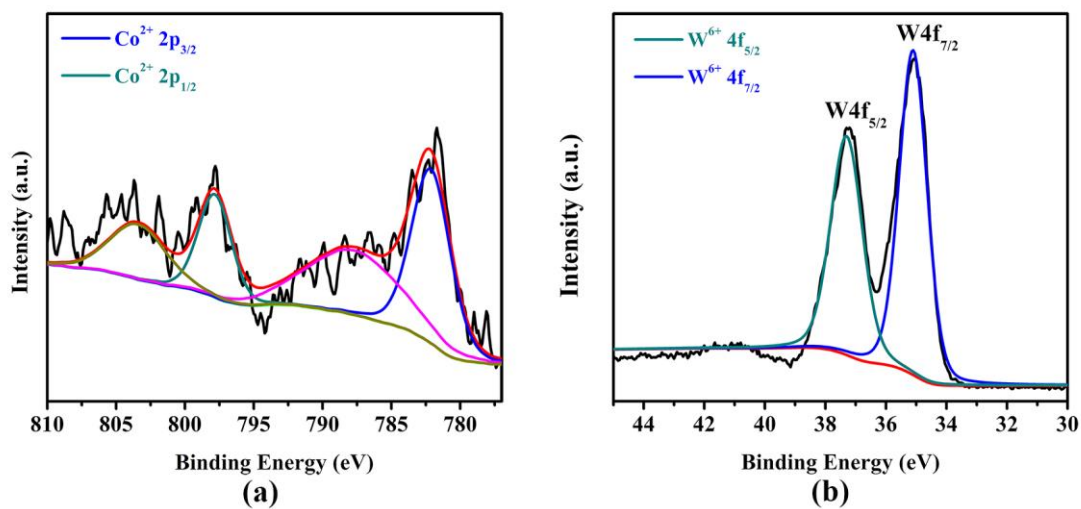


Figure S7 XPS spectra of compound 2: (a) Co; (b) W.

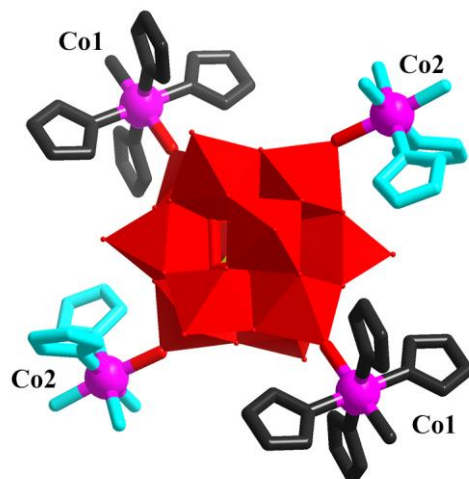


Figure S8 The coordination environment of BW_{12} (the four connected node) anion in compound 2.

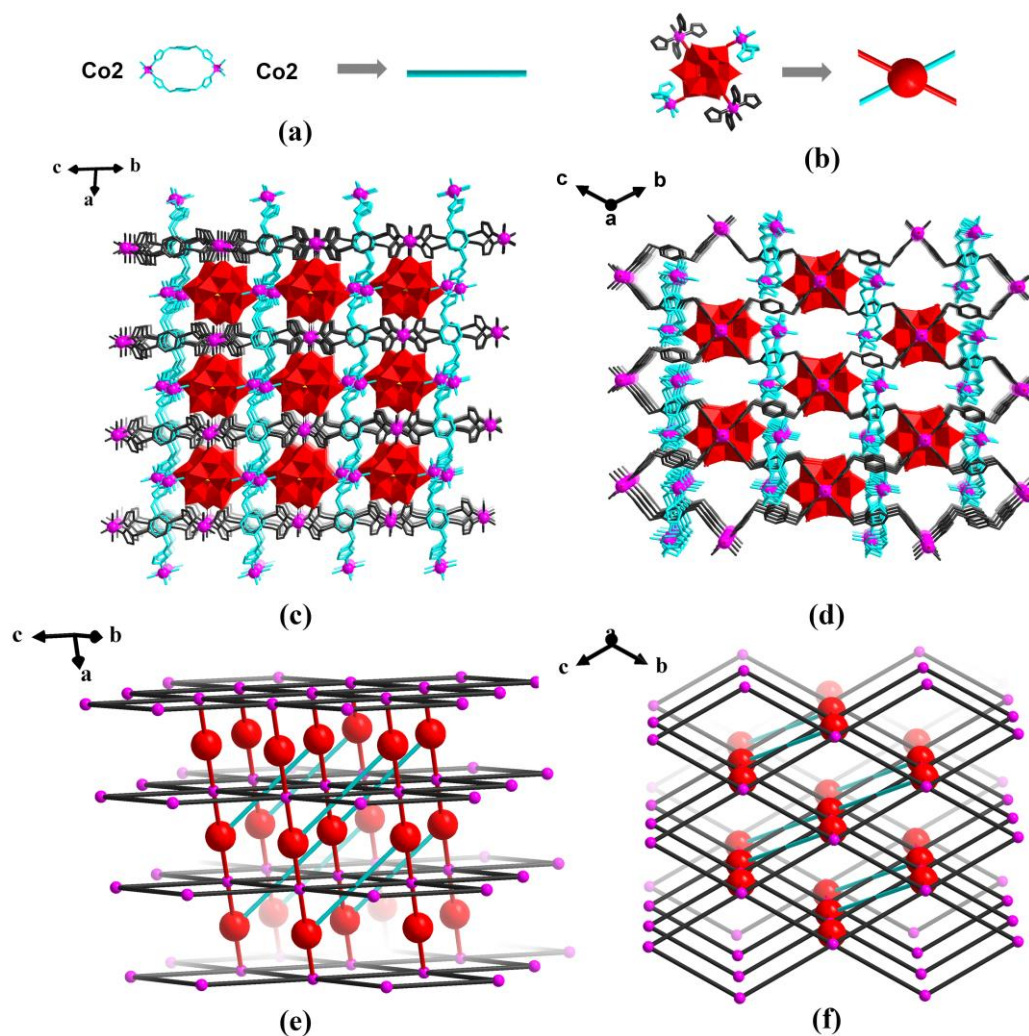


Figure S9 (a) and (b) the scheme view of 0D loops and POMs in compound 2; (c) and (d) Polyhedral and ball-and-stick views of POM-supported 3-D network in compound 2 viewed along different axis; (e) and (f) the scheme view of 4,6T19 topology in compound 2 along different direction.

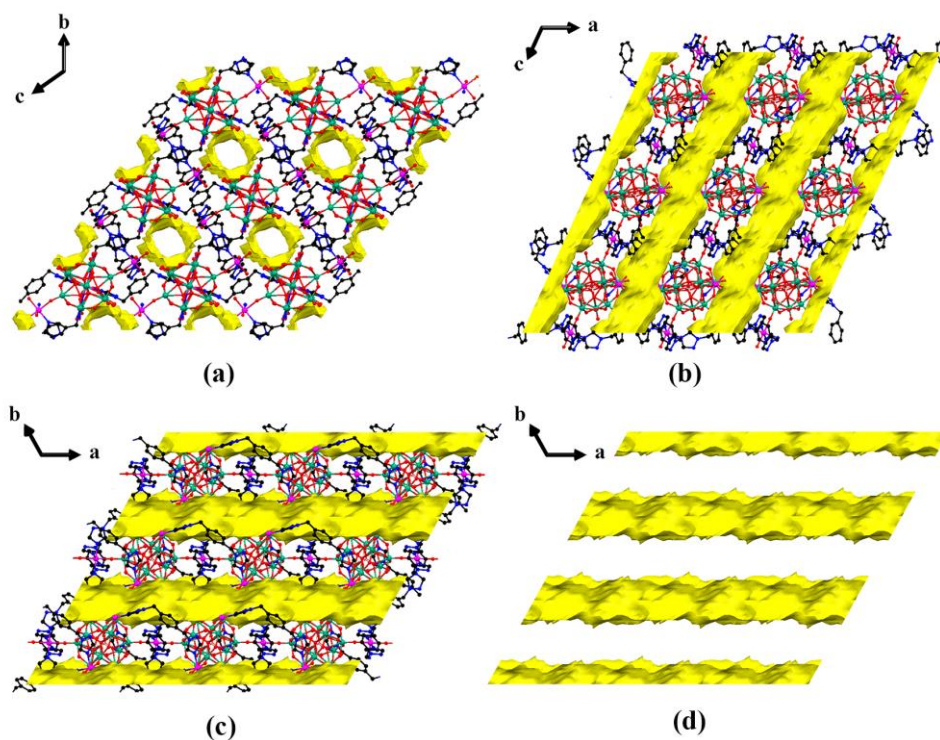


Figure S10 (a-d) Packing arrangement of compound 2, in which the solvent accessible voids in the channels are modeled with yellow background: (a) viewed along [100] direction (a axis); (b) viewed along b axis; (c) and (d) viewed along c axis.

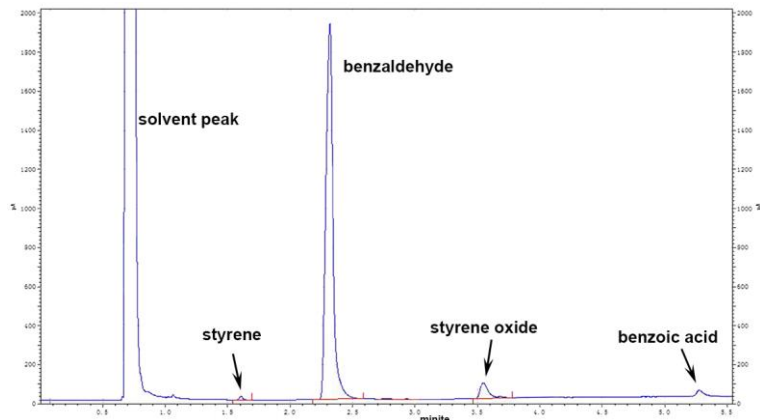


Figure S11 The corresponding GC result of styrene oxidation catalyzed by compound 1.

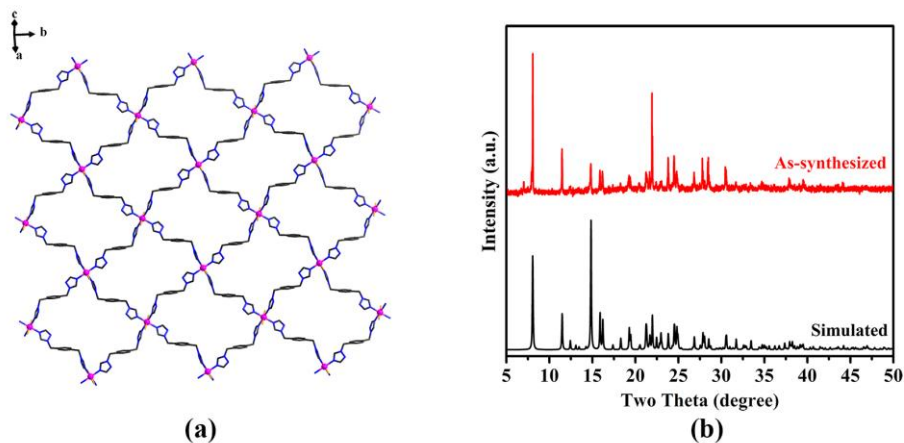


Figure S12 (a) Polyhedral and ball-and-stick views of $\text{Co}(\text{BBTZ})_2\text{Cl}_2$; (b) The Powder X-ray diffraction patterns of $\text{Co}(\text{BBTZ})_2\text{Cl}_2$, which demonstrate that the peak position of simulated and as-synthesized samples are in agreement with each other, indicating the good phase purity.

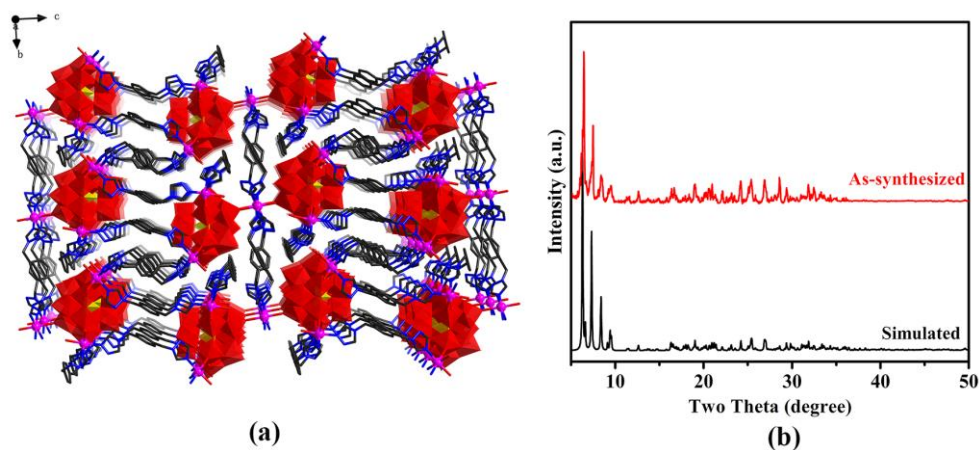


Figure S13 (a) Polyhedral and ball-and-stick views of the POM-supported 3D network of $[\text{Co}_{2.5}(\text{bbtz})_4(\text{H}_2\text{O})][\text{BW}_{12}\text{O}_{40}] \cdot 4\text{H}_2\text{O}$; (b) The Powder X-ray diffraction patterns of $[\text{Co}_{2.5}(\text{bbtz})_4(\text{H}_2\text{O})][\text{BW}_{12}\text{O}_{40}] \cdot 4\text{H}_2\text{O}$, which show that the peak position of simulated and as-synthesized compound 3 are in agreement with each other, indicating the good phase purity.

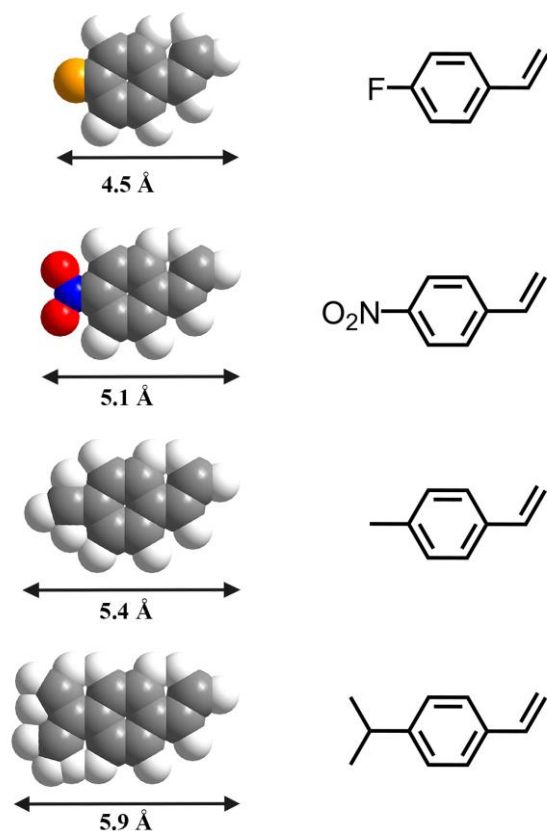


Figure S14 The different molecular size of substrates.

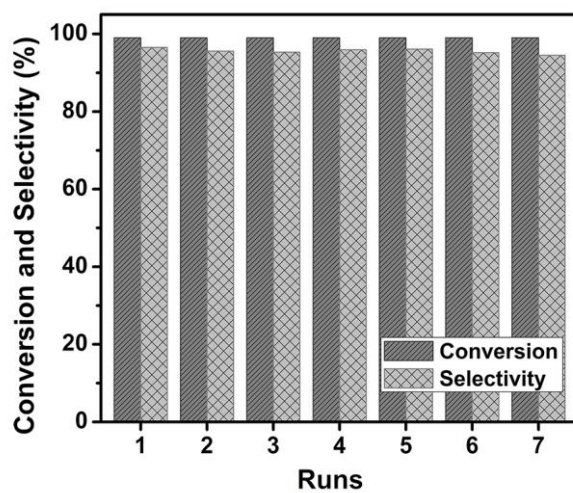


Figure S15 The recycle experiments with compound 1 as catalyst. The results demonstrate that the activity and selectivity of compound 1 could be maintained after seven cycles.

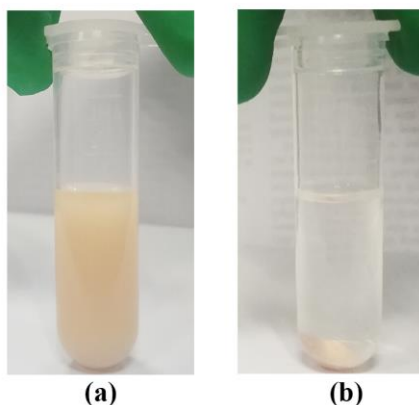


Figure S16 Compound 1 as the heterogeneous catalyst dispersed in reaction system (left photo) and recycled by the simple centrifugal separation (right photo).

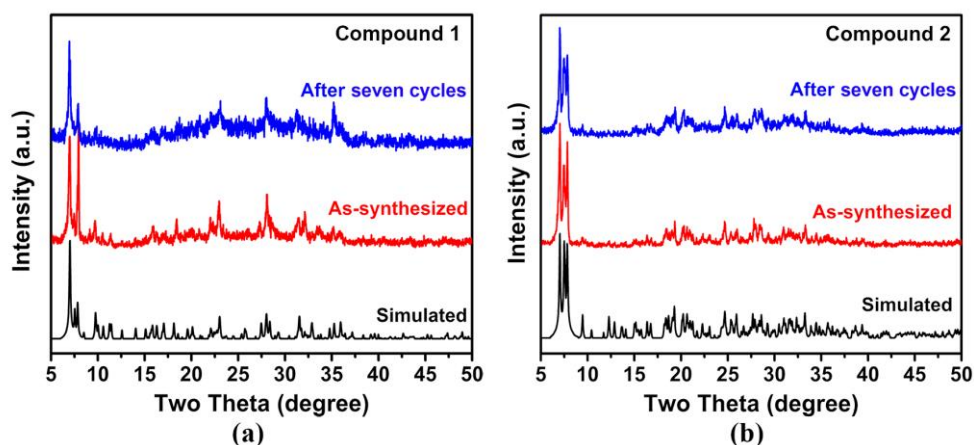


Figure S17 (a) and (b) The PXRD patterns of compound 1 and compound 2 before catalysis and after seven cycles. The results indicate that compound 1 and 2 have good structural stability and the structures could be maintained after the catalytic reaction.

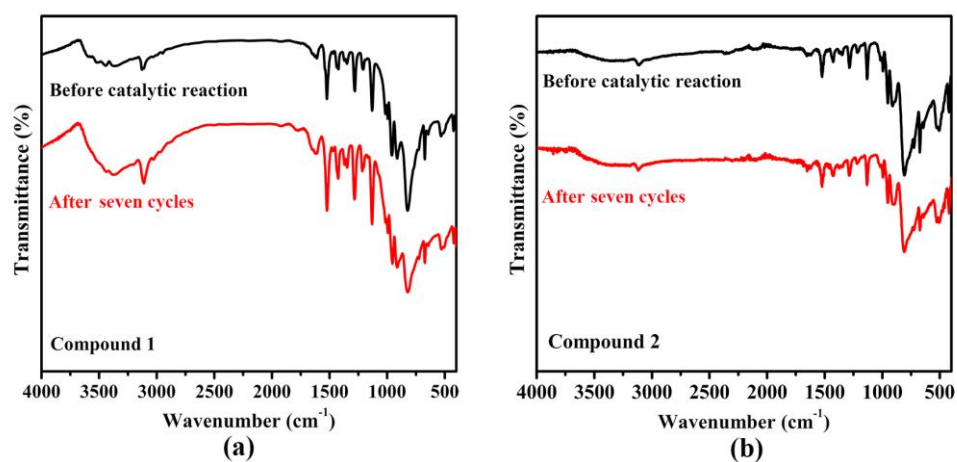


Figure S18 (a) and (b) The IR spectrum of compound 1 and compound 2 before catalysis and after seven cycles.

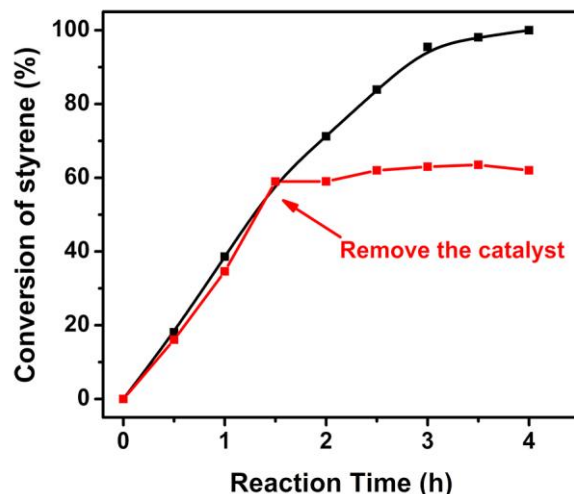


Figure S19 Leaching test with compound 1 as catalyst for selective oxidation of styrene.

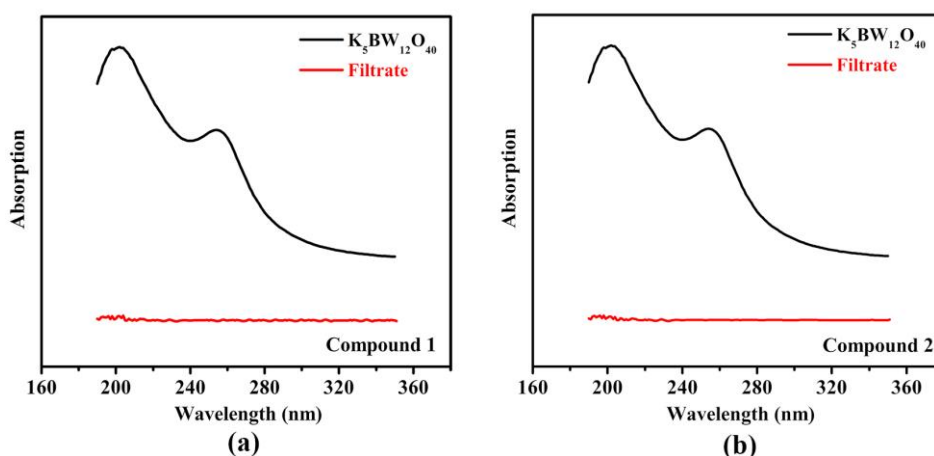


Figure S20 (a-b) UV-vis absorption spectra of $K_5[BW_{12}O_{40}]$ (black) and the filtrate (red) after removing compound 1 (a) and compound 2 (b). These results suggest that no signals of the characteristic peaks of $K_5[BW_{12}O_{40}]$ can be observed in the filtrate, indicating the heterogeneity of compound 1 and 2.

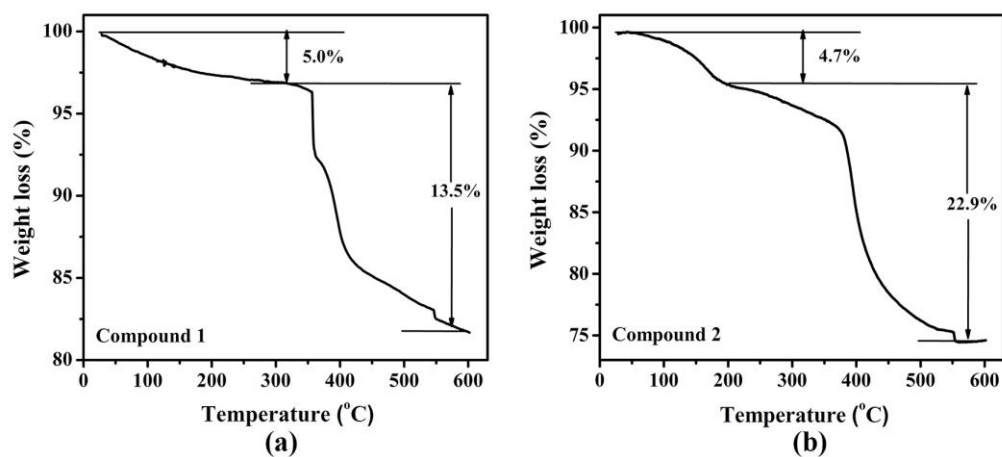


Figure S21 (a-b) The TG curves of compound 1 and 2. Both of compound 1 and 2 display

two-step weight loss. The first weight loss corresponds to the loss of eleven lattice and/or coordinated water molecules, and the second weight loss is ascribed to the decomposition of ligands.

4. Supplementary tables for compounds 1 and 2.

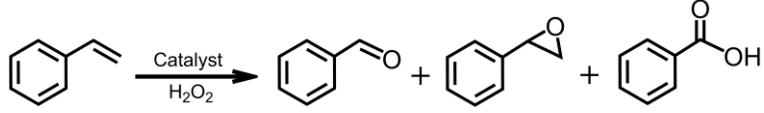
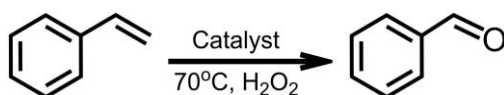
Table S1. Selective oxidation of styrene with various polyoxometalates. ^[a]			
			
Entry	Catalysts	Conversion (%) ^[b]	Selectivity for benzaldehyde (%) ^[b]
1	Na ₂ HPMo ₁₂ O ₄₀	35±4	81±2
2	Na ₃ PW ₁₂ O ₄₀	53±2	60±2
3	K ₄ SiW ₁₂ O ₄₀	48±3	69±3
4	K ₅ BW ₁₂ O ₄₀	51±2	89±2
^[a] Reaction conditions: styrene (0.25 mmol), H ₂ O ₂ (1 mmol), catalysts (0.028 mmol), acetonitrile (2 ml), 70 °C, reaction time: 12 h. ^[b] The values are based on GC analysis.			

Table S2. Selected bond lengths (Å) and angles (deg) of compound 1.			
Co(1)-N(1)	2.112(13)	Co(1)-N(4)#3	2.143(14)
Co(1)-N(1)#2	2.112(13)	Co(1)-N(4)#4	2.143(14)
Co(1)-O(7)	2.181(15)	Co(1)-O(7)#2	2.181(15)
N(1)-Co(1)-N(1)#2	180.0	N(1)-Co(1)-N(4)#4	88.9(6)
N(1)-Co(1)-N(4)#3	91.1(6)	N(1)-Co(1)-O(7)#2	89.8(6)
N(1)-Co(1)-O(7)	90.2(6)		
Symmetry transformations used to generate equivalent atoms: #1 -x, +y, 3/2-z; #2 -x+1/2, -y+3/2, -z+2; #3 1-x, 2-y, 2-z; #4 -1/2+x, -1/2+y, +z.			

Table S3. The bond-valence sum (BVS) calculations of W and Co for compound 2. ^[a]			
Atom	oxidation states	Atom	oxidation states
W (1)	6.67	Co (1)	2.15
W (2)	6.25	Co (2)	2.25
W (3)	6.16		
W (4)	6.10		
W (5)	6.16		
W (6)	6.26		
^[a] The bond-valence sum (BVS) calculation method is according Ref. [2].			

Table S4. Selected bond lengths (Å) and angles (deg) of compound 2 .			
Co(1)-N(10)	2.149(8)	Co(1)-N(7)	2.166(8)
Co(1)-N(10)#2	2.149(8)	Co(1)-N(7)#2	2.166(8)
Co(1)-O(2)	2.155(8)	Co(1)-O(2)#2	2.155(8)
Co(2)-N(1)	2.144(9)	Co(2)-N(4)#3	2.145(10)
Co(2)-O(18)	2.156(15)	Co(2)-O(1W)	2.120(10)
Co(2)-O(2W)	2.041(11)	Co(2)-O(3W)	2.163(18)
N(10)-Co(1)-N(10)#2	180.0(0)	N(10)-Co(1)-N(7)	88.8(4)
N(10)-Co(1)-N(7)#2	91.2(4)	N(10)-Co(1)-O(2)#2	89.1(3)
N(10)-Co(1)-O(2)	90.9(3)	N(1)-Co(2)-O(2W)	175.9(4)
N(1)-Co(2)-N(4)#3	95.9(6)	N(1)-Co(2)-O(1W)	90.3(4)
N(1)-Co(2)-O(3W)	91.4(5)	N(1)-Co(2)-O(18)	90.5(4)
Symmetry transformations used to generate equivalent atoms: #1 -x+1,-y+1,-z+1; #2 -x,-y+1,-z+1; #3 -x+2,-y+1,-z+2.			

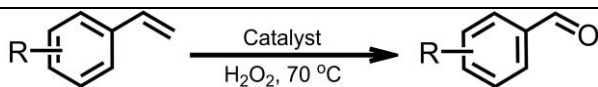
Table S5. Selective oxidation of styrene catalyzed by compound 1 with various amounts of H₂O₂.^[a]



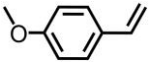
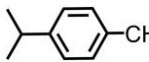
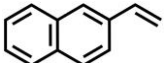
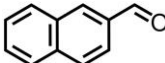
Entry	Amount of H ₂ O ₂ (mmol)	Conversion (%) ^[b]	Selectivity for benzaldehyde (%) ^[b]
1	0.5	70±4	95±4
2	1.0	100	96±3
3	2.0	100	75±3

^[a] Reaction conditions: styrene (0.25 mmol), H₂O₂, compound 1 (0.028 mmol), acetonitrile (2 ml), 70 °C, reaction time: 4 h. ^[b] The values are based on GC analysis.

Table S6. Selective catalytic oxidation of styrene derivatives to the corresponding aldehydes with H₂O₂.^[a]

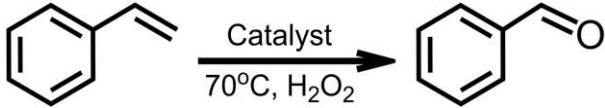


Entry	Substrate	Product	Time (h)	Compound 2 ^[b]	
				Conversion	Selectivity
1			6	>99	93
2			6	>99	97
3			9	94	96.2
4			9	95	97.8
5			9	91	98.9

6			10	94	95
7			10	95	96
8			10	90	94

^[a] Reaction conditions: styrene derivatives (0.25 mmol), H₂O₂ (1 mmol), compound 2 (0.028 mmol), solvent (2 ml), 9 h. ^[b] Determined by GC analysis.

Table S7. The comparison of catalytic performance of POMOF catalysts and various other reported catalysts for the styrene oxidation into benzaldehyde.

						
Entry	Catalyst	Oxidant	Reaction conditions	Conv. /%	Select. /%	Reference
1	Compound 1	H ₂ O ₂	70 °C, in CH ₃ CN, 4h	100	96	This work
2	SiW ₁₁ Co@ aptesSBA-15	H ₂ O ₂	80 °C, in CH ₃ CN, 24h	100	75	Ref. [3]
3	Cs ₅ [PCo(H ₂ O) Mo ₁₁ O ₃₉]·6H ₂ O	H ₂ O ₂	80 °C, 10h	98.9	97.1	Ref. [4]
4	PW ₁₁ Zn-APTES@SiO ₂	H ₂ O ₂	70 °C, in CH ₃ CN, 24h	100	54	Ref. [5]
5	{Co ₂ Zn ₃ W ₁₉ }	H ₂ O ₂	50 °C, in CH ₃ CN, 12h	98	94	Ref. [6]
6	NbCoS	H ₂ O ₂	70 °C, 48h	96.4	73.7	Ref. [7]
7	PMA@MC-2	TBHP, O ₂	70 °C, 24h	92	55	Ref. [8]
8	CuO/Co ₃ O ₄	TBHP	70 °C, in CH ₃ CN, 10h	100	84	Ref. [9]
9	Fe-SNP	H ₂ O ₂	reflux, water, 4h	100	95	Ref. [10]

5. Reference:

- [1] (a) Sheldrick, G. M. SHELXS-97, *Program for solution of crystal structures*, University of Göttingen, Germany, **1997**; (b) Sheldrick, G. M. SHELXL-97, *Program for refinement of crystal structures*, University of Göttingen, Germany, **1997**.
- [2] Brown, I. B.; Altermatt, D. Bond-valence parameters obtained from a systematic analysis of the Inorganic crystal structure database. *Acta Crystallogr. Sect B.* **1976**, *32*, 1957-1960.
- [3] Balula, S. S.; Cunha-Silva, L.; Santos, I. C. M. S.; Estrada, A. C.; Femandes, A. C.; Cavaleiro, J. A. S.; Pires, J.; Freire, C.; Cavaleiro, A. M. V. Mono-substituted silicotungstates as a active catalysts for sustainable oxidations: homo- and heterogeneous performance. *New J. Chem.*, **2013**, *37*, 22350.
- [4] Pathan, S.; Patel, A. Transition-metal-substituted phosphomolybdates: catalytic and kinetic study for liquid-phase oxidation of styrene. *Ind. Eng. Chem. Res.* **2013**, *52*, 11913-11919.
- [5] Nogueira, L. S.; Ribeiro, S.; Granadeiro, C. M.; Pereira, E.; Feio, G.; Cunha-Silva, L.; Balula, S. S. Novel polyoxometalate silica nano-sized spheres: efficient catalysts for olefin oxidation and the deep desulfurization process. *Dalton Trans.*, **2014**, *43*, 9518-9528.
- [6] Tang, J.; Yang, X. L.; Zhang, X. W.; Wang, M.; Wu, C. D. A functionalized polyoxometalate solid for selective oxidation of styrene to benzaldehyde. *Dalton Trans.*, **2010**, *39*, 3396-3399.
- [7] Parvulescu, V.; Constantin, C.; Su, B. L. Liquid phase oxidation of aromatic hydrocarbons using highly ordered Nb and NbCo-MCM-41 nanoreactors. *J. Mol. Catal. A*, **2003**, *202*, 171-178.
- [8] Chilivery, R.; Rana, R. K. Microcapsule structure with a tunable textured surface via the assembly of polyoxometalate clusters: a bioinspired strategy and enhanced activities in alkene oxidation. *ACS Appl. Mater. Interfaces* **2017**, *9*, 3161-3167.
- [9] Ge, D. H.; Wang, J. Q.; Geng, H. B.; Lu, S. L.; Wang, D. T.; Li, X. M.; Zhao, X. L.; Cao, X. Q.; Gu, H. W. Facile synthesis of copper-based metal oxide nanoparticles with exceptional catalytic activity for the selective oxidation of styrenes into benzaldehydes. *ChemplusChem*, **2014**, *80*, 511-515.
- [10] Rajabi, F.; Karimi, N.; Saidi, M. R.; Primo, A.; Varma, R. S.; Luque, R. Unprecedented selective oxidation of styrene derivatives using a supported iron oxide nanocatalyst in aqueous medium. *Adv. Synth. Catal.*, **2012**, *354*, 1707-1711.